

Journal Pre-proofs

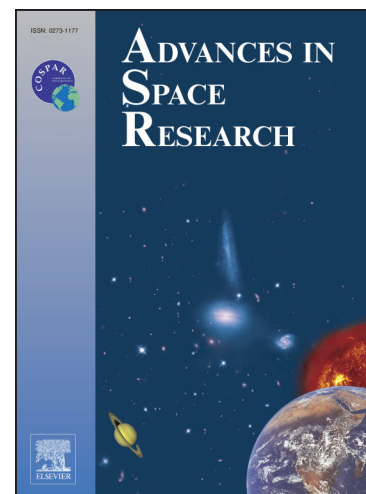
Assessment and exploitation of coastal Low Resolution Mode sea level data from CryoSat-2 on the entrance to the Gulf of California

Jonathan Valle-Rodríguez, Jesús Gómez-Enri, Armando Trasviña-Castro

PII: S0273-1177(23)00696-8
DOI: <https://doi.org/10.1016/j.asr.2023.08.048>
Reference: JASR 16934

To appear in: *Advances in Space Research*

Received Date: 24 April 2023
Revised Date: 24 August 2023
Accepted Date: 28 August 2023



Please cite this article as: Valle-Rodríguez, J., Gómez-Enri, J., Trasviña-Castro, A., Assessment and exploitation of coastal Low Resolution Mode sea level data from CryoSat-2 on the entrance to the Gulf of California, *Advances in Space Research* (2023), doi: <https://doi.org/10.1016/j.asr.2023.08.048>

This is a PDF file of an article that has undergone enhancements after acceptance, such as the addition of a cover page and metadata, and formatting for readability, but it is not yet the definitive version of record. This version will undergo additional copyediting, typesetting and review before it is published in its final form, but we are providing this version to give early visibility of the article. Please note that, during the production process, errors may be discovered which could affect the content, and all legal disclaimers that apply to the journal pertain.

Assessment and exploitation of coastal Low Resolution Mode sea level data from CryoSat-2 on the entrance to the Gulf of California

Jonathan Valle-Rodríguez^a, Jesús Gómez-Enri^b, Armando Trasviña-Castro^c

^aEnvironmental Hydraulics Institute “IH Cantabria”, Universidad de Cantabria, C/Isabel Torres n°15, Parque Científico y Tecnológico de Cantabria, 39011 Santander, Spain

^bApplied Physics Department, University of Cadiz, Av. República Saharaui, s/n, Puerto Real, Cádiz 11510, Spain

^cCentro de Investigacion Cientifica de Educacion Superior de Ensenada, Unidad La Paz (CICESE-ULP), C. Miraflores 334, Bella Vista, 23050, La Paz, Baja California Sur, México

Corresponding author: Jonathan Valle-Rodríguez, jonathan.valle@unican.es

Abstract

The CryoSat-2 mission (CS2), initially conceived for sea ice measurements, is also useful for sea level monitoring in oceanic and coastal areas. Only specific regions have two high resolution modes (SAR Delay/Doppler and SAR-Interferometric modes), while the rest of the areas are measured in low-resolution mode (LRM). The entrance to the Gulf of California presents this mode of operation. Sea Level Anomalies (SLA) obtained from CS2 are compared with tide gauges at three locations, Cabo San Lucas (CSL) south of the Baja California peninsula, Mazatlán (MZ) and San Blas (SB) on the continental margin. The comparison shows good agreement between SLAs in CSL and MZ, with standard deviations of the differences (SDD) lower than 0.09 m and Pearson’s correlations higher than 0.7 (95% of confidence level). San Blas is in a complex location and with less data, presenting an SDD greater than 0.13 m and a correlation below 0.55. We present the cross-shore seasonal and interannual variability in CSL and MZ using the CS2 SLA time series from 2011 to 2020. The variability shows the presence of events such as El Niño (2015 to early 2016), La Niña (2011) and the warm event of 2014 (nicknamed “the Blob”). Additionally, the residual time series of CS2 obtained after extracting the annual, semi-annual and monthly components, shows the East side (at MZ) is more affected by El Niño/La Niña variability while the West side (at CSL) is more influenced by the Blob/El Niño. Estimated long-term SLA trend at both locations are around 3.1 mm/yr, supporting similar findings by previous studies.

Keywords: Coastal altimetry, sea level anomaly, tide gauges, CryoSat-2.

1. Introduction

The CryoSat-2 mission (CS2, hereinafter) was launched in April 2010 carrying the SIRAL (Synthetic Aperture Radar and Interferometric Radar Altimeter) instrument, with the main goal of measuring the thickness and variation of sea ice in the polar region (Wingham et al., 2006; Boufard et al., 2018). The orbit of this mission is quasi-geodetic, with a repetition cycle of around 369 days (with a 30-days sub-cycle), capable of making a large number of measurements (5344 revolutions) reaching latitudes up to 88° (Boufard et al., 2017). Initially the mission was conceived to have a lifetime of 3.5 years (Parrinello et al., 2018); however, it remains in activity until the current date making this mission such a great success.

CryoSat-2 can measure in three different modes, the low-resolution mode (LRM), and two high-resolution modes, the Delay/Doppler SAR (Synthetic Aperture Radar) mode that improves the resolution along-track and the SARIn mode (SAR interferometric) that receives the signal from a second antenna in the across-track direction allowing better identification of the location of the echo (Parrinello et al., 2018; ESA – ESRIN, 2019). The modes operate according to a geographical mode mask. The current mode mask (v4.0) is shown in ESA – ESRIN (2019). Following this mask, the SAR mode operates on sea ice and some oceanographic areas, the SARIn mode measures on ice sheet margins, mountains, and glaciers; while the LRM mode covers most of the oceanic and coastal areas, continental ice sheets and areas not covered by the other modes.

Several studies validate SAR and SARIn measurements in coastal areas by comparing them with in-situ sea level from tide gauges. Fenoglio et al. (2015) validate the sea surface heights (SSH) from SAR in the German Bight and find standard deviations of the differences (SDD) of 8 cm. Gómez-Enri et al. (2017) find good agreements between Sea Level Anomalies (SLA) obtained from SAR data and tide gauge in the coastal strip of 3 - 20 km respect to the coastline over the eastern platform of the Gulf of Cadiz (Iberian Peninsula), they also indicate that SAR measurements can be affected by complex morphologies and river discharges. Dinardo et al. (2018) mention that terrestrial contamination affects the SAR sea level measurements at 2-3 km from the coast. Idzanović et al. (2018) compare SLA from SARIn data with tide gauges over the coast of Norway and find better results when using local ocean tide and inverted barometer corrections, obtaining SDD of 12 cm and correlations of 68%. Labroue et al. (2012) carry out the first assessment of LRM data (20 Hz) from CS2 and despite the small amount of data analyzed, they show that this mission is useful in oceanic studies of significant wave height (SWH) and SLA. Calafat et al. (2017) also evaluate and validate SLA and SWH from LRM data against in-situ observations from tide gauges, buoys and Argo floats, showing great performance of CS2 over the ocean comparable to the Jason-2 mission.

One of the main challenges when validating the SLAs obtained from CS2 is the choice of the tidal model that best resolves the main tidal components in our region and the proper use of the corrective term Sea State Bias (SSB). The first is evaluated following the analysis described in Oreiro et al. (2014) from which the TPX09 model (Egbert and Erofeeva, 2002) was chosen. The analysis is detailed in the supplementary material. The corrective term SBB is different for each altimetric mission since it depends on the wind speed and SWH, however during the CS2 data processing the wind speed is not computed and only a reference value is used (7 m/s), therefore

the SSB obtained depends mainly on the SWH (Labroue et al., 2012). The works of Fenoglio et al. (2015), Gómez-Enri et al. (2017) and Dinardo et al. (2018) have used around 5% SWH instead of SSB as a first approximation. In this work, a wider range (0 to 20% SWH) is tested to find the percentage that provides better results when compared to in-situ data.

The aforementioned studies validate CS2 data in its different modes in oceanic and some coastal regions, however many coastal areas, where only LRM mode is available, remain without validation. In this paper we validate the SLAs obtained from the LRM mode in coastal areas against in-situ tide gauges of the entrance to the Gulf of California, considering local ocean tide corrections and, instead of the sea state bias available in the altimeter product, we use a percentage of the SWH. This is particularly interesting if one considers the amount of LRM data from this satellite that are still unexploited in ocean and coastal zones. In fact, more than 50% of coastal areas are under LRM mode. Once validated we use SLAs from CS2 to describe the seasonality and other oceanographic phenomena, such as El Niño, on the coastal zone in the period from 2011 to 2020. This paper is organized as follows. Section 2 describes the study area and dataset used here. Section 3 is dedicated to the methodology, while Section 4 shows the results and Section 5 the discussion. Finally, Section 6 presents conclusions.

2. Study area and dataset

2.1 Physical conditions

The entrance to the Gulf of California (EGC, Fig. 1c) is in direct communication with the Eastern Tropical Pacific Ocean and from there it receives the seasonal sea level signal, with maximum in summer and minimum in winter, as reported by Ripa (1997) using tide gauge data, and Strub and James (2002a) using altimetry data. The region is also characterized by the interaction of three surface water masses (Portela et al., 2016) that vary with the seasonal circulation (Wyrтки, 1965; Baumgartner and Christensen, 1985). Cold waters of the California Current arrive at the EGC from the western margin of the Baja California peninsula (Fig. 1a) in winter and early spring, with geostrophic velocities around 0.2 m/s (Durazo, 2015; Valle and Trasviña, 2017). During summer and autumn, the Mexican Coastal Current (MCC) (Badan-Dangon, 1998) brings warm tropical waters from the south over the continental margin (east side of Fig.1c) and into the Gulf of California. Lavin et al. (2006) report geostrophic velocities ~ 0.3 m/s associated with the MCC, and that can be reinforced by the passage of a coastal trapped wave (Zamudio et al., 2007, 2008). In addition, around the tip of the peninsula (Fig. 1a), a coastal current is generated and propagates poleward over the west side of the peninsula (Valle and Trasviña, 2017). The wind is another physical forcing in this region and presents a monsoonal behavior, from the NW in winter (8 m/s) and from the SE in the summer (< 5 m/s) influencing the surface circulation accordingly (Badan-Dangon et al., 1991, 2003; Marinone et al., 2004). Remote events such as ENSO (El Niño-Southern Oscillation) cause higher sea level values (Strub and James, 2002b), while La Niña produces the opposite effect.

2.2 Bathymetry and coastal morphology

The region presents a wide continental shelf on the mainland side and a narrow on the Baja California peninsula (Fig. 1). Figure 1c shows this feature by plotting the bathymetry to 2000 m. In the central zone, depths reach > 3000 m. Coastal land relief can interfere with the altimetry radar

contaminating the return signal and complicating the retracking of geophysical parameters (Gommenginger et al., 2011). In the first 2 – 4 km of the coastal plain around the tide gauge in Cabo San Lucas (Fig. 1a), heights are 100 m or less, increasing inland to about 900 m. Near Mazatlán (Fig. 1b) most of the coastal area has elevations smaller than 100 m. In the area around San Blas (Fig. 1d), there are hills > 200 m in height to the southeast of the tide gauge near the coast that can interfere with the radar signal. The bathymetries are obtained from the General Bathymetric Chart of the Oceans (GEBCO, <https://www.gebco.net/>) and the elevations from Terra Advanced Spaceborne Thermal Emission and Reflection Radiometer (ASTER) Global Digital Elevation Model (GDEM) Version 3 (ASTGTM, <https://lpdaac.usgs.gov/products/astgtmv003/>).

2.3 Dataset

- CryoSat-2 data

CryoSat-2 data is distributed by the European Space Agency (ESA) and is freely available for download at <ftp://science-pds.cryosat.esa.int>. We use level 2 GOP (Geophysical Ocean Product) data distributed 30 days after data acquisition. The satellite tracks are shown with gray lines in Fig. 1. For our location, only data in low-resolution mode (LRM) at 20 Hz is available (approximately 350 m between consecutive measurements). For now, a coastal retracker has not been used for this altimetric mission, so we use the processed LRM data accordingly to Maximum Likelihood Estimator (MLE4) retracker (Amarouche et al., 2004). The purpose of using MLE4 is to evaluate the official product distributed and estimate how close to the shore we can find acceptable measurements of this mission. CryoSat-2 GOP products are taken for the period from 2011 to 2020. A more detailed description of the data is found in Parrinello et al. (2018) and Bouffard et al. (2018).

- Tide gauge data

Tide gauge locations in the EGC are represented by purple circles in Fig. 1. The first one is in Cabo San Lucas (CSL) and is located at the tip of the Baja California peninsula. Records in CSL are distributed by the sea level network of the Center for Scientific Research and Higher Education of Ensenada (CICESE, <http://redmar.cicese.mx/>) with a sampling interval of 1 minute. The other two tide gauge stations are located on the continental coast, Mazatlán (MZ) and San Blas (SB). Both present hourly sea level records and are provided by the Secretary of the Navy of Mexico (SEMAR, <https://oceanografia.semar.gob.mx/estaciones.html>). Due to data gaps, the period available for each station is different, so we consider records from 2011 to 2016 for MZ and SB, and until mid-2017 for CSL. The gaps are the reason why the CICESE data is divided into two periods (Fig. 2a), while the hourly data (Fig. 2b and 2c) present gaps of days, weeks or months.

3. Methodology

Due to the long repetition period of CS2 (369 days), the comparison with tide gauges is made with tracks that fall within an area centered around the tide gauge (Calafat et al., 2017; Gómez-Enri et al., 2017; Idžanović et al., 2018). In our study we choose a radius of 0.5 degrees around each tide gauge and keep measurements within 40 km from the coastline and then form sea level anomaly time series as a function of distance from the coastline. The reference coastline is shown in red in Figures 1a, 1b and 1d. Because the SB tide gauge is in a semi-enclosed area, and to avoid

duplicate measurements, the reference coastline at this location is mainly composed of the section to the north of the tide gauge. After choosing the tracks, we obtain and compare the sea level anomalies (SLA) from both CS2 and the tide gauges. The SLA of CS2 is obtained following Eq. (1).

$$SLA_{CS2} = \textit{Altitude} - \textit{Range} - \textit{Iono} - \textit{Dry} - \textit{Wet} - \textit{MSS} - \textit{PTi} - \textit{SET} - \textit{Tide}^* - \textit{DAC} - \textit{SSB}^{**} \quad (1)$$

where *Altitude* is the distance between the satellite's center of mass and the reference ellipsoid (WGS84). The retracked *Range* is the distance between the satellite and the mean reflected surface. *Iono* is for ionospheric correction from Global Ionospheric Maps developed by NASA/JPL (Mannucci et al., 1998). *Dry* and *Wet* correspond to tropospheric corrections. *Dry* is obtained from the European Centre for Medium-Range Weather Forecasts (ECMWF) model and *Wet* (Path Delay Plus, GPD+) is developed and validated by the University of Porto (Fernandez and Lazaro, 2016). Mean Sea Surface (*MSS*) is from the CNES_CLS-15 product based on 20 years of altimetric data, distributed by AVISO+ (<https://www.aviso.altimetry.fr/en/data/products/auxiliary-products/mss.html>). *PTi* and *SET* are pole tide (Wahr, 1985) and solid earth tide (Cartwright and Eden, 1973) respectively. *Tide** represents the astronomical tide based on 8 tidal components ($M_2, S_2, K_2, N_2, P_1, O_1, K_1, Q_1$), obtained for each CS2 track from the TPXO9v4 model (Egbert and Erofeeva, 2002). This model was chosen because it shows a better performance to solve the tide in our study area (see supplementary material). Dynamic atmospheric correction (*DAC*) combines the effects of high-frequency dynamic ocean response to atmospheric forcing (Carrère and Lyard, 2003) and inverted barometer effects. The maximum and minimum values of the geophysical corrections for the three local areas in Fig. 1 are shown in Table 1 in the supplementary material.

*SSB*** is the sea state bias correction. We replace the *SSB* available in the product (based on Tran et al., 2012) by a percentage of the significant wave height (SWH) as a first approximation, following Fenoglio-Marc et al. (2015) and Gómez-Enri et al. (2017). The SWH represents the average wave height of one-third largest waves in a particular geographic location (ESA-ESRIN, 2019). In this work, a percentage of 0 - 20% SWH (added negatively) is evaluated to obtain a better comparison with the tide gauge sea level anomalies. Previously, we removed the outliers in the SWH using the median absolute deviation (MAD), following Passaro et al., 2021. This analysis is performed in blocks of 20 values where SWH values are considered valid if:

$$x < \textit{median}(X) + 3 \cdot \textit{MAD}(X) \quad \textit{or} \quad x > \textit{median}(X) - 3 \cdot \textit{MAD}(X) \quad (2)$$

$$\textit{MAD}(X) = 1.4286 \cdot \textit{median}(|X - \textit{median}(X)|) \quad (3)$$

where x are the individual values of SWH within the block of 20 values (X). Additionally, a threshold maximum of 10 m is established for the SWH values.

For SLAs, we perform two screenings. The first is based on Gómez-Enri et al. (2017) where we keep the SLA values within the range [-1.5 to 1.5] m for each track. Since we only choose the values in the first 40 km from the coast, the SLAs should not exceed the median ± 3 times the standard deviation. Values outside this criterion are considered outliers. A second screening is performed on the SLA time series formed at each kilometer with respect to the coastline. To obtain an SLA point at each kilometer, we average the values that are present in that interval, considering that the data at 20 Hz from CS2 correspond to measurements every ~ 350 m. The value at 1km is the average of the SLAs from the coastline to the first kilometer from the coastline and

so on with the other positions. With the positions defined at each kilometer, the SLA time series is formed and a threshold of the mean value ± 2.5 times the standard deviation is applied. The value of 2.5 times the standard deviation was obtained after a comparison with the SLAs of the tide gauges in CSL and MZ. In the case of SB, this value was close to 3, due to less data for comparison. With this second step, we eliminate most of the highest anomalous values remaining after the first screening. The SLAs for the tide gauge data are obtained using Eq. (4).

$$SLA_{TG} = Nm - Tide^* - DAC \quad (4)$$

Where Nm corresponds to sea level record. For the tides ($Tide^*$), the same model TPXO9v4 is used and the tidal components are obtained for the times closest to the CS2 passes. In the case of hourly tide gauge data, we choose the sea level value within 30 min or less around the CS2 pass. The DAC is taken from AVISO+ (<https://www.aviso.altimetry.fr/en/data/products/auxiliary-products/dynamic-atmospheric-correction.html>). This correction is obtained after spatially and temporally interpolating the regular 6-hours gridded maps to the position of the tide gauge and the near times of the altimetric passes of CS2.

To obtain a residual SLA time series and consequently estimate trends, we extract the annual (SA, 365.2 days), semi-annual (SSA, 182.6 days) and monthly (MM, 27.5 days) signals from the SLA time series through a harmonic analysis following the model in Thomson and Emery (2014):

$$x(t) = \bar{x} + \sum_{q=1}^3 [A_q \cos(2\pi f_q t) + B_q \sin(2\pi f_q t)] + x_r(t) \quad (5)$$

where \bar{x} is the mean value of the record; x_r is the residual of the time series and A_q, B_q are the coefficients to be determined for each harmonic. Finally, a linear fit is applied to the residual time series (x_r) whose slope is the value of the trend.

4. Results

4.1 Determination of best %SWH for SSB correction

Sea Level Anomalies time series of CS2 (SLA_{CS2}) and tide gauges (SLA_{TG}) are compared considering a percentage of 0 to 20% of the significant wave height (SWH) for SLA_{CS2} (as a first approximation of the SSB). The SLAs of both datasets are comparable after extracting the temporal average over the same evaluation period. To determine the percentage of SWH that allows a greater similarity between both SLA time series, we calculate the standard deviation of the differences (SDD) and correlation between both time series.

Figure 3 shows the root mean square (Rms) of the SDD and correlation with respect to the percentage of the SWH. The best percentage for Cabo San Lucas (CSL, left plot) is 7% SWH, however it can be used from 5 to 8% without obtaining great differences. For Mazatlán location (MZ, right plot), the best percentage is 9% SWH, but it is also possible to use from 7 to 10%. In both cases, when 10% SWH is exceeded, the SDD between SLA_{CS2} and SLA_{TG} increases, and the correlations decrease significantly. Because San Blas (SB) presents a smaller amount of comparison points between the tide gauge and CS2 (almost half that in the other two locations), a percentage of 8% SWH was taken according to the analysis made in the other two locations.

Once the %SWH for each location is determined (7%, 9%, and 8% for CSL, MZ, and SB, respectively), we estimate the percentage of SLA values that remain after the two screening steps with respect to the distance to coast (Fig. 4). The first 3 km of CSL (Fig. 4a) and MZ (Fig. 4b) show percentages less than 80% while SB (Fig. 4c) is less than 50%. CSL maintains around 90% of SLA values at distances greater than 9 km. MZ presents around 85% at distances greater than 10 km and SB only presents percentages greater than 80% at 15 km from the coastline. Based on these results, we only consider the time series of SLA_{C2} that present more than 80% of values for CSL (from 4 km) and 75% for locations of MZ and SB (4 and 5 km respectively). A similar percentage is found in Birol et al. (2021) using data from Jason1-3 missions and processed with ALES retracker and X-TRACK software, where altimetry points with more than 80% of SLA values are saved.

4.2 Validation of SLA time series

To determine the positions with respect to the coast where the lowest standard deviations of the differences (SDD) and high correlations are obtained, we compared the SLA time series from tide gauge (SLA_{TG}) and CS2 (SLA_{CS2}). Note that 7%, 9% and 8% SWH were applied to the CSL, MZ and SB locations, respectively in Eq. 1. For CSL (Fig. 5) the positions between 10 to 14 km present the lowest SDD (0.05 - 0.06 m), while the correlations in those positions range between 0.8 and 0.85. At greater distances, the SDD (correlations) gradually increase (decrease) but remain smaller (greater) than 0.08 m (0.7). The same is observed closer to the coast in the [4 – 10] km coastal band. The reason to this might be related to the fact of not being using a coastal-dedicated retracker. Even if the data quality is good in the [4-10] km coastal strip (Fig. 4), the MLE is not well adapted to retrack accurately the retracked range used in Eq. 1. The SLA_{TG} and SLA_{C2} time series at 11 km for CSL (Fig. 6), show the lowest SDD (0.05 m) and the highest correlation (0.85). At this distance from the coastline, SDD and correlation calculations are made based on one hundred comparison points, almost 2 measurements per month for the period of analysis. Both SLA series range from -0.2 to 0.2 m.

At the MZ location, the lowest SDD is found from 8 km to 12 km (0.07 – 0.08 m), with correlations between 0.8 – 0.85 (Fig. 7). At other positions with respect to the coastline, the SDDs range from 0.075 to 0.09 m while the correlations exceed 0.73. At 9 km, both time series present the lowest SDD (0.074) and high correlation (0.84). The similarity between both series is remarkable even during El Niño event in 2015, although with higher values for CS2 (Fig. 8). Sea Level Anomalies in this location range between ± 0.3 m. The statistics (SDD and correlation) are obtained from 71 comparison points, approximately a monthly measurement. This is due to the fact that there are many gaps in the SLA series of the tide gauge, as shown in Fig. 2b.

As mentioned before, the SB location presents few comparison values, due to gaps in the tide gauge series and a lower number of CS2 passes within a semi-closed area. Standard deviation of the difference (SDD) values (Fig. 9 top) is higher than 0.14 m in the first 15 km respect to the coastline. At greater distances they range between 0.13 – 0.14 m. The correlations (Fig. 9 bottom) improve from 15 km but remain less than 0.55. The SLA_{TG} and SLA_{CS2} time series are not plotted here because the existing values are not sufficient for an adequate qualitative comparison.

4.3 Seasonality and other oceanographic phenomena as observed by CS2

A broad view of the SLA distribution obtained from CS2 data is presented using Hovmöller diagrams for the CSL (Fig. 10 top) and MZ (Fig. 10 middle) locations. These are built with all tracks available in the study area between 2011 and 2020 close to the coast: [0 – 40] km of track segment. The bottom panel of Figure 10 includes a plot of the MEI index (Multivariate ENSO Index, <https://psl.noaa.gov/enso/mei/>). Although the MEI does not use fixed symmetric thresholds to determine the strength of ENSO (El Niño – Southern Oscillation) events, it considers that values greater (lower) than 2 (-2) can be flagged as strong El Niño (La Niña) events (Wolter and Timlin, 2011).

The diagrams allow to appreciate the seasonality of the SLAs in both locations, with marked characteristic. From 2011 to mid-2012 the region is affected by the final phase of a strong La Niña event of 2010, and from mid-2015 to early 2016 the signal corresponds to a strong El Niño event (Fig. 10 bottom). During La Niña, the SLAs in CSL (Fig 10 top) vary between -0.15 to 0.15 m, while in MZ (Fig 10 middle) the variability is larger (-0.25 to 0.25 m). Godinez et al (2010) and Farach-Espinoza et al. (2021) report that the influence of ENSO in the entrance to the Gulf of California is larger in eastern coastal areas, as in MZ, and that under strong El Niño and La Niña conditions, seasonal variability is more relevant. In both locations there is an extension of the period of negative anomalies. During El Niño, the positive anomalies intensify reaching SLAs greater than 0.3 m in both locations, as for instance in 2015. The years with low positive MEI index, from mid-2018 to beginning 2020, suggest normal conditions or a weak El Niño event. However, both locations present high and long-lasting SLAs with values less than 0.3 m. In the summer of 2014, a strong positive seasonal signal is appreciated in both locations, which coincides with the effects of a warm event nicknamed "the Blob" (Bond et al., 2015). This event started with positive temperature anomalies off the Gulf of Alaska, spreading to the coastal areas of southern California during the spring of 2014 (Leising et al., 2015). The arrival of this event is more evident in CSL due to its northern origin and maintains positive SLAs with values close to 0.3 m until the end of the year.

To get the trends in both locations we first calculate an average of the SLAs of the first 40 km of each track over the respective location and from the years 2011 – 2020. These are presented in the Figures 11a/12a for CSL/MZ (red line). The blue line in these figures are the reconstructed signals of the three harmonics in both locations, while the residuals are shown in Fig. 11b and Fig. 12b. Trends are estimated after performing a linear fit to the SLA residuals. The residual SLA series (black line) reveals that the effects of the final phase of La Niña in 2011 are more noticeable in CSL than MZ. Comparing Fig 11b and 12 b, values at the end of the 2011 reach -200 mm in CSL and only -150 mm in MZ. Similarly, during the beginning of La Niña 2020, the negative SLAs are more pronounced in MZ, with peaks between -150 to -250 mm, while at CSL they only reach -100 mm. On the other hand, during strong El Niño event from 2015 to mid-2016, both locations clearly show similar positive impact on residual SLAs, with maximums around 200 mm, only with more variability in MZ. Nguyen et al. (2022) mention that warm/cool events such as El Niño/La Niña generally have effects on sea level rise, increasing/decreasing the sea level, although the relationship is not always direct in all events. For instance, in 2018, while MZ presents high positive residual SLA (> 100 mm), at CSL negative residuals occur most of the year and only change at the end of the year. This happens when conditions change from La Niña to normal or weak El Niño event (blue and red shaded areas in Fig. 11b and Fig. 12b). Positive SLA residuals also occur in 2014, associated to the Blob (Bond et al., 2015). During this warm event, values are as high as those during El Niño 2015 event. At CSL one peak >200 mm happened in mid-2014 and another

near 200 mm at the end of the year. In contrast at MZ, only the first peak greater than 200 mm was registered. The effects of the Blob in our study area are still under investigation.

The purple lines in Fig 11b and 12 b are the sea level trends estimated from 10 years of CS2 data. They show a sea level rise of 3.1 ± 1.4 mm/yr at CSL and 3.1 ± 1.6 mm/yr at MZ. In comparison, global trends based on the longer periods show a broader picture of trends including marked changes in recent years. For instance, 3.35 ± 0.4 mm/yr based on the period from 1993 to 2017 (Ablain et al., 2019) and 3.55 ± 0.4 mm/yr for the period from 1993 to October 2022 estimated by AVISO (<https://www.aviso.altimetry.fr/msl/>, accessed on 06 January 2023). In coastal areas, Cazenave et al. (2022) show similar trends to those found here near the coastline and on the period 2002 - 2019. However, trends may be higher, as in the case of North Java, where the trend in the first 50 km is 3.8 ± 2.6 mm/yr, based on the period from 2003 to 2014 (Passaro et al., 2016) or near the island of Hon Dau in Vietnam, with 7.38 mm/yr for the years between 2001 to 2020 (Nguyen et al., 2022). A longer time series is necessary, merging CS2 with other satellite altimetric missions, to corroborate the trends found here and also to decrease the uncertainties, as in the work of Ablain et al. (2019).

5. Discussion and conclusions

Many factors can affect the quality and quantity of SLA data obtained from altimetry missions in coastal zones. One of them is the retracker that is used to obtain the range and SWH. For CS2 data in LRM mode only the MLE4 retracker is available in the official product. We must also consider the orientation of the tracks with respect to the coastline. When the satellite approaches the coast, the power signal received by the altimeter (waveforms) will have less land contamination if approaching in an orthogonal direction (Dinardo et al., 2011). Likewise, the complex coastal morphology also limits the amount of data that can be recovered, as shown in the study area of Idzanović et al. (2018). In our study, the San Blas (SB) location (Fig. 1d) presents a lower amount of data recovered because it is in a semi-enclosed area and some tracks to the southeast of the tide gauge are more susceptible to land-contamination.

Other factors are the corrections applied to the range to obtain the SLAs, such as the sea state bias (SSB) which is different for each altimetric mission being related to the altimetric design and processing (Labroue et al., 2012). However, it is also possible to use a percentage of SWH as a first approximation. Fenoglio-Marc et al. (2015) and Gómez-Enri et al. (2017) use 5% SWH while Dinardo et al. (2018) uses 4.7%. Here we tested from 0 to 20% SWH and found that in our study area 7 to 9 % give the best results when comparing against in-situ measurements. Another important correction applied to obtain the SLA is the tide, which by default (in level 2 data) comes from the FES2014 global tidal model (Lyard et al., 2021). The choice of a tidal model depends on its performance over a specific study area and may be different from the model used in the official product. Thus, for example, Dinardo et al. (2018) uses the TPXO8 model (Egbert and Erofeeva, 2002) for the tidal correction in the German Bight and West Baltic Sea. Gómez-Enri et al. (2017) use the DTU10 model (Cheng and Andersen, 2011) in the eastern continental shelf of the Gulf of Cadiz. We use an improved version of the Egbert and Erofeeva model (TPXO9v4, released in December 2020), chosen after carrying out an analysis with tide gauges over the study area (see supplementary material), following Oreiro et al. (2014). Also, the number of tidal constituents that need to be extracted in the study area vary from 8 to 15 (see Table 7 in Valle and Trasiña, 2020).

Additionally, the analysis made by Lyard et al. (2021) emphasizes the good performance of TPX09 model in coastal areas and platforms, where this study is focused.

After applying corrections to the range and obtaining the SLAs, and implementing outlier detection steps to keep the best quality data, as explained in section 3, we proceed to evaluate the usefulness of the CS2 SLAs in LRM mode by comparing them with those obtained from tide gauges. Our results indicate a good performance of CS2 in the areas of CSL and MZ with SDD less than 0.09 m and correlations greater than 0.7. In contrast, at the SB location we obtained larger SDDs (> 0.13 m) and smaller correlations (< 0.55), however, it is possible with the CS2 mission to obtain SLA values in coastal areas with many limitations and that is not densely measured by other altimetric missions as CS2 does.

The SLA variability obtained from Hovmöller diagrams allow to describe the seasonality as well as interannual variability, such as the SLA intensification or attenuation produced by the El Niño/La Niña, or the Blob, in the 40 km coastal band at the entrance to the Gulf of California (the CSL and MZ sites). Although the effects of strong La Niña of 2010 are not completely registered in this study, the period covered by our analysis includes the final phase of La Niña 2010-2011, and the beginning of the long La Niña 2020-2023, while the Blob of 2014 and the strong El Niño of 2015 are fully captured. The response at both locations presents a direct relationship when the events are moderate or strong, with greater variability in MZ, and the response can differ when remote forcing is weak or absent.

The estimated trends based on ten years of CS2 SLA data are similar in both locations (3.1 mm/yr) and close to the regional trends estimated by AVISO (3.55 mm/yr). Ablain et al. (2019) mention an acceleration of 0.12 mm/yr^2 in the global mean sea level, however we need a longer SLA time series to be able to verify that such acceleration is taking place in our study area.

We conclude that the data in the LRM mode of the CS2 mission can be useful in coastal areas even when they have not been processed with a coastal retracker, reaching acceptable values (in terms of accuracy) up to 4 km from the coastline, allowing us to study the seasonal and interannual variability of sea level in coastal areas of the Mexican Pacific. The percentage of SWH used instead the SSB correction is a little higher than in other studies, which suggests that it is necessary to identify an appropriate threshold of this percentage in the validation stage, using in-situ data at the study region. Future works may use CS2 data in other coastal regions where LRM is available and unexploited, considering limitations that may exist in those specific regions. The continuity of this mission is ensured with the future Copernicus Polar Ice and Snow Topography Altimeter (CRISTAL), planned for launch in 2027.

Acknowledgements

The CryoSat-2 altimetry data used in this study were distributed by European Space Agency. Sea level records were provided by the sea level network of the Center for Scientific Research and Higher Education of Ensenada (CICESE, <http://redmar.cicese.mx/>) and the Secretary of Navy of Mexico (SEMAR, <https://oceanografia.semar.gob.mx/estaciones.html>).

References

- Ablain, M., Legeais, J.F., Prandi, P., Marcos, M., Fenoglio-Marc, L., Dieng, H.B., Benveniste, J. and Cazenave, A., 2017. Satellite altimetry-based sea level at global and regional scales. In *Integrative study of the mean sea level and its components* (pp. 9-33). Springer, Cham.
<https://doi.org/10.1007/s10712-016-9389-8>
- Ablain, M., Meyssignac, B., Zawadzki, L., Jugier, R., Ribes, A., Spada, G., Benveniste, J., Cazenave, A. and Picot, N., 2019. Uncertainty in satellite estimates of global mean sea-level changes, trend and acceleration. *Earth System Science Data*, 11(3), pp.1189-1202. <https://doi.org/10.17882/58344>
- Amarouche, L., Thibaut, P., Zanife, O.Z., Dumont, J.P., Vincent, P. and Steunou, N., 2004. Improving the Jason-1 ground retracking to better account for attitude effects. *Marine Geodesy*, 27(1-2), pp.171-197. <https://doi.org/10.1080/01490410490465210>
- Andersen, O.B. and Scharroo, R., 2011. Range and geophysical corrections in coastal regions: and implications for mean sea surface determination. In *Coastal altimetry* (pp. 103-145). Springer, Berlin, Heidelberg. https://doi.org/10.1007/978-3-642-12796-0_5
- Badan-Dangon, A., Dorman, C.E., Merrifield, M.A. and Winant, C.D., 1991. The lower atmosphere over the Gulf of California. *Journal of Geophysical Research: Oceans*, 96(C9), pp.16877-16896.
<https://doi.org/10.1029/91JC01433>
- Badan-Dangon, A., 1998. Coastal Circulation from the Galápagos to the Gulf of California, The Sea, vol. 11, The Global Coastal Ocean, Regional Studies and Syntheses, edited by AR Robinson and KH Brink, pp. 315–343, John Wiley, Hoboken, N. J.
- Badan, A., 2003. The atmosphere over the Gulf of California. In *Nonlinear Processes in Geophysical Fluid Dynamics* (pp. 205-212). Springer, Dordrecht. https://doi.org/10.1007/978-94-010-0074-1_12
- Baumgartner, T.R. and Christensen, N., 1985. Coupling of the Gulf of California to large-scale interannual climatic variability. *Journal of Marine Research*, 43(4), pp.825-848.
<https://doi.org/10.1357/002224085788453967>
- Biol, F., Léger, F., Passaro, M., Cazenave, A., Niño, F., Calafat, F.M., Shaw, A., Legeais, J.F., Gouzenes, Y., Schwatke, C. and Benveniste, J., 2021. The X-TRACK/ALES multi-mission processing system: New advances in altimetry towards the coast. *Advances in Space Research*, 67(8), pp.2398-2415. <https://doi.org/10.1016/j.asr.2021.01.049>
- Bond, N.A., Cronin, M.F., Freeland, H. and Mantua, N., 2015. Causes and impacts of the 2014 warm anomaly in the NE Pacific. *Geophysical Research Letters*, 42(9), pp.3414-3420.
<https://doi.org/10.1002/2015GL063306>
- Bouffard, J., Naeije, M., Banks, C.J., Calafat, F.M., Cipollini, P., Snaith, H.M., Webb, E., Hall, A., Mannan, R., Féménias, P. and Parrinello, T., 2018. CryoSat ocean product quality status and future evolution. *Advances in Space Research*, 62(6), pp.1549-1563.
<https://doi.org/10.1016/j.asr.2017.11.043>

- Calafat, F.M., Cipollini, P., Bouffard, J., Snaith, H. and Féménias, P., 2017. Evaluation of new CryoSat-2 products over the ocean. *Remote Sensing of Environment*, 191, pp.131-144. <https://doi.org/10.1016/j.rse.2017.01.009>
- Carrère, L. and Lyard, F., 2003. Modeling the barotropic response of the global ocean to atmospheric wind and pressure forcing-comparisons with observations. *Geophysical Research Letters*, 30(6). <https://doi.org/10.1029/2002GL016473>
- Cartwright, D.E. and Edden, A.C., 1973. Corrected tables of tidal harmonics. *Geophysical journal international*, 33(3), pp.253-264. <https://doi.org/10.1111/j.1365-246X.1973.tb03420.x>
- Cazenave, A., Gouzenes, Y., Birol, F., Leger, F., Passaro, M., Calafat, F.M., Shaw, A., Nino, F., Legeais, J.F., Oelmann, J. and Restano, M., 2022. Sea level along the world's coastlines can be measured by a network of virtual altimetry stations. *Communications Earth & Environment*, 3(1), p.117. <https://doi.org/10.1038/s43247-022-00448-z>
- Cheng, Y. and Andersen, O.B., 2011. Multimission empirical ocean tide modeling for shallow waters and polar seas. *Journal of Geophysical Research: Oceans*, 116(C11). <https://doi.org/10.1029/2011JC007172>
- Cipollini, P., Calafat, F.M., Jevrejeva, S., Melet, A. and Prandi, P., 2017. Monitoring sea level in the coastal zone with satellite altimetry and tide gauges. *Integrative Study of the Mean Sea Level and Its Components*. Space Sciences Series of ISSI, vol 58, pp.35-59. Springer, Cham. https://doi.org/10.1007/978-3-319-56490-6_3
- Dinardo, S., Fenoglio-Marc, L., Buchhaupt, C., Becker, M., Scharroo, R., Fernandes, M.J. and Benveniste, J., 2018. Coastal sar and plrm altimetry in german bight and west baltic sea. *Advances in Space Research*, 62(6), pp.1371-1404. <https://doi.org/10.1016/j.asr.2017.12.018>
- Durazo, R., 2015. Seasonality of the transitional region of the California Current System off Baja California. *Journal of Geophysical Research: Oceans*, 120(2), pp.1173-1196. <https://doi.org/10.1002/2014JC010405>
- Egbert, G.D. and Erofeeva, S.Y., 2002. Efficient inverse modeling of barotropic ocean tides. *Journal of Atmospheric and Oceanic technology*, 19(2), pp.183-204. [https://doi.org/10.1175/1520-0426\(2002\)019<0183:EIMOBO>2.0.CO;2](https://doi.org/10.1175/1520-0426(2002)019<0183:EIMOBO>2.0.CO;2)
- ESA-ESRIN, 2019. Baseline-C CryoSat Ocean Processor, Ocean Product Handbook Version 4.1. European Space Agency, Frascati, Italy. Available at: <https://earth.esa.int/eogateway/documents/20142/37627/CryoSat-Baseline-C-Ocean-Product-Handbook.pdf>
- Farach-Espinoza, E.B., López-Martínez, J., García-Morales, R., Nevárez-Martínez, M.O., Lluch-Cota, D.B. and Ortega-García, S., 2021. Temporal variability of oceanic mesoscale events in the Gulf of California. *Remote sensing*, 13(9), p.1774. <https://doi.org/10.3390/rs13091774>
- Fenoglio-Marc, L., Dinardo, S., Scharroo, R., Roland, A., Sikiric, M.D., Lucas, B., Becker, M., Benveniste, J. and Weiss, R., 2015. The German Bight: A validation of CryoSat-2 altimeter data in

- SAR mode. *Advances in Space Research*, 55(11), pp.2641-2656.
<https://doi.org/10.1016/j.asr.2015.02.014>
- Fernandes, M.J. and Lázaro, C., 2016. GPD+ wet tropospheric corrections for CryoSat-2 and GFO altimetry missions. *Remote Sensing*, 8(10), p.851. <https://doi.org/10.3390/rs8100851>
- Godínez, V.M., Beier, E., Lavín, M.F. and Kurczyn, J.A., 2010. Circulation at the entrance of the Gulf of California from satellite altimeter and hydrographic observations. *Journal of Geophysical Research: Oceans*, 115(C4). <https://doi.org/10.1029/2009JC005705>
- Gómez-Enri, J., Vignudelli, S., Cipollini, P., Coca, J. and González, C.J., 2017. Validation of CryoSat-2 SIRAL sea level data in the eastern continental shelf of the Gulf of Cadiz (Spain). *Advances in Space Research*, 62(6), pp.1405-1420. <https://doi.org/10.1016/j.asr.2017.10.042>
- Gommenginger, C., Thibaut, P., Fenoglio-Marc, L., Quartly, G., Deng, X., Gómez-Enri, J., Challenor, P. and Gao, Y., 2011. Retracking altimeter waveforms near the coasts. *Coastal altimetry*, pp.61-101. https://doi.org/10.1007/978-3-642-12796-0_4
- Idžanović, M., Ophaug, V. and Andersen, O.B., 2018. Coastal sea level from CryoSat-2 SARIn altimetry in Norway. *Advances in Space Research*, 62(6), pp.1344-1357.
<https://doi.org/10.1016/j.asr.2017.07.043>
- Labroue, S., Boy, F., Picot, N., Urvoy, M. and Ablain, M., 2012. First quality assessment of the Cryosat-2 altimetric system over ocean. *Advances in Space Research*, 50(8), pp.1030-1045.
<https://doi.org/10.1016/j.asr.2011.11.018>
- Lavín, M.F., Beier, E., Gómez-Valdés, J., Godínez, V.M. and García, J., 2006. On the summer poleward coastal current off SW México. *Geophysical Research Letters*, 33(2).
<https://doi.org/10.1029/2005GL024686>
- Leising, A.W., Schroeder, I.D., Bograd, S.J., Abell, J., Durazo, R., Gaxiola-Castro, G., Bjorkstedt, E.P., Field, J., Sakuma, K., Robertson, R.R. and Goericke, R., 2015. State of the California Current 2014-15: Impacts of the Warm-Water" Blob". *California Cooperative Oceanic Fisheries Investigations Reports*, 56.
- Lyard, F.H., Allain, D.J., Cancet, M., Carrère, L. and Picot, N., 2021. FES2014 global ocean tide atlas: design and performance. *Ocean Science*, 17(3), pp.615-649. <https://doi.org/10.5194/os-17-615-2021>
- Mannucci, A.J., Wilson, B.D., Yuan, D.N., Ho, C.H., Lindqwister, U.J. and Runge, T.F., 1998. A global mapping technique for GPS-derived ionospheric total electron content measurements. *Radio science*, 33(3), pp.565-582. <https://doi.org/10.1029/97RS02707>
- Marinone, S.G., Parés-Sierra, A., Castro, R. and Mascarenhas, A., 2004. Correction to "Temporal and spatial variation of the surface winds in the Gulf of California". *Geophysical Research Letters*, 31(10). <https://doi.org/10.1029/2004GL020064>

- Nguyen, H.M., Ouillon, S. and Vu, V.D., 2022. Sea Level Variation and Trend Analysis by Comparing Mann–Kendall Test and Innovative Trend Analysis in Front of the Red River Delta, Vietnam (1961–2020). *Water*, 14(11), p.1709. <https://doi.org/10.3390/w14111709>
- Oreiro, F.A., D'Onofrio, E., Grismeyer, W., Fiore, M. and Saraceno, M., 2014. Comparison of tide model outputs for the northern region of the Antarctic Peninsula using satellite altimeters and tide gauge data. *Polar Science*, 8(1), pp.10-23. <https://doi.org/10.1016/j.polar.2013.12.001>
- Parrinello, T., Shepherd, A., Bouffard, J., Badessi, S., Casal, T., Davidson, M., Fornari, M., Maestroni, E. and Scagliola, M., 2018. CryoSat: ESA's ice mission—Eight years in space. *Advances in Space Research*, 62(6), pp.1178-1190. <https://doi.org/10.1016/j.asr.2018.04.014>
- Passaro, M., Dinardo, S., Quartly, G.D., Snaith, H.M., Benveniste, J., Cipollini, P. and Lucas, B., 2016. Cross-calibrating ALES Envisat and CryoSat-2 Delay–Doppler: a coastal altimetry study in the Indonesian Seas. *Advances in Space Research*, 58(3), pp.289-303. <https://doi.org/10.1016/j.asr.2016.04.011>
- Passaro, M., Hemer, M.A., Quartly, G.D., Schwatke, C., Dettmering, D. and Seitz, F., 2021. Global coastal attenuation of wind-waves observed with radar altimetry. *Nature Communications*, 12(1), pp.1-13. <https://doi.org/10.1038/s41467-021-23982-4>
- Portela, E., Beier, E., Barton, E.D., Castro, R., Godínez, V., Palacios-Hernández, E., Fiedler, P.C., Sánchez-Velasco, L. and Trasviña, A., 2016. Water masses and circulation in the tropical Pacific off central Mexico and surrounding areas. *Journal of Physical Oceanography*, 46(10), pp.3069-3081. <https://doi.org/10.1175/JPO-D-16-0068.1>
- Ray, C., Martin-Puig, C., Clarizia, M.P., Ruffini, G., Dinardo, S., Gommenginger, C. and Benveniste, J., 2015. SAR altimeter backscattered waveform model. *IEEE Transactions on Geoscience and Remote Sensing*, 53(2), pp.911-919. <https://doi.org/10.1109/TGRS.2014.2330423>
- Ripa, P., 1997. Toward a Physical Explanation of the Seasonal Dynamics and Thermodynamics of the Gulf of California. *Journal of physical oceanography*, 27(5), pp.597-614. [https://doi.org/10.1175/1520-0485\(1997\)027<0597:TAPEOT>2.0.CO;2](https://doi.org/10.1175/1520-0485(1997)027<0597:TAPEOT>2.0.CO;2)
- Strub, P.T. and James, C., 2002a. Altimeter-derived surface circulation in the large–scale NE Pacific Gyres.: Part 1. seasonal variability. *Progress in Oceanography*, 53(2-4), pp.163-183. [https://doi.org/10.1016/S0079-6611\(02\)00029-0](https://doi.org/10.1016/S0079-6611(02)00029-0)
- Strub, P.T. and James, C., 2002b. The 1997–1998 oceanic El Niño signal along the southeast and northeast Pacific boundaries—An altimetric view. *Progress in Oceanography*, 54(1-4), pp.439-458. [https://doi.org/10.1016/S0079-6611\(02\)00063-0](https://doi.org/10.1016/S0079-6611(02)00063-0)
- Thomson, R.E. and Emery, W.J., 2014. *Data analysis methods in physical oceanography*. Elsevier Science, 3rd edition, pp. 728. <https://doi.org/10.1016/C2010-0-66362-0>
- Tran, N., Philipps, S., Poisson, J.-C., Urien, S., Bronner, E., Picot, N., 2012. Impact of GDR-D standards on SSB corrections. OSTST, 22–29 September, 2012 Venice, Italy. Available at https://www.aviso.altimetry.fr/fileadmin/documents/OSTST/2012/oral/02_friday_28/01_instr_processing_I/01_IP1_Tran.pdf.

Valle-Rodríguez, J. and Trasviña-Castro, A., 2017. Poleward currents from coastal altimetry: The west coast of Southern Baja California, Mexico. *Advances in Space Research*, 59(9), pp.2313-2324. <https://doi.org/10.1016/j.asr.2017.01.050>

Valle-Rodríguez, J. and Trasviña-Castro, A., 2020. Sea level anomaly measurements from satellite coastal altimetry and tide gauges at the entrance of the Gulf of California. *Advances in Space Research*, 66(7), pp.1593-1608. <https://doi.org/10.1016/j.asr.2020.06.031>

Wahr, J.M., 1985. Deformation induced by polar motion. *Journal of Geophysical Research: Solid Earth*, 90(B11), pp.9363-9368. <https://doi.org/10.1029/JB090iB11p09363>

Wingham, D.J., Francis, C.R., Baker, S., Bouzinac, C., Brockley, D., Cullen, R., de Chateau-Thierry, P., Laxon, S.W., Mallow, U., Mavrocordatos, C. and Phalippou, L., 2006. CryoSat: A mission to determine the fluctuations in Earth's land and marine ice fields. *Advances in Space Research*, 37(4), pp.841-871. <https://doi.org/10.1016/j.asr.2005.07.027>

Wolter, K. and Timlin, M.S., 2011. El Niño/Southern Oscillation behaviour since 1871 as diagnosed in an extended multivariate ENSO index (MEI. ext). *International Journal of Climatology*, 31(7), pp.1074-1087. <https://doi.org/10.1002/joc.2336>

Wyrtki, K., 1965. Surface currents of the eastern tropical Pacific Ocean. Inter-American Tropical Tuna Commission Bulletin. Vol. IX, No. 5, 268-305.

Zamudio, L., Hurlburt, H.E., Metzger, E.J. and Tilburg, C.E., 2007. Tropical wave-induced oceanic eddies at Cabo Corrientes and the Maria Islands, Mexico. *Journal of Geophysical Research: Oceans*, 112(C5). <https://doi.org/10.1029/2006JC004018>

Zamudio, L., Hogan, P. and Metzger, E.J., 2008. Summer generation of the Southern Gulf of California eddy train. *Journal of Geophysical Research: Oceans*, 113(C6). <https://doi.org/10.1029/2007JC004467>

Figures

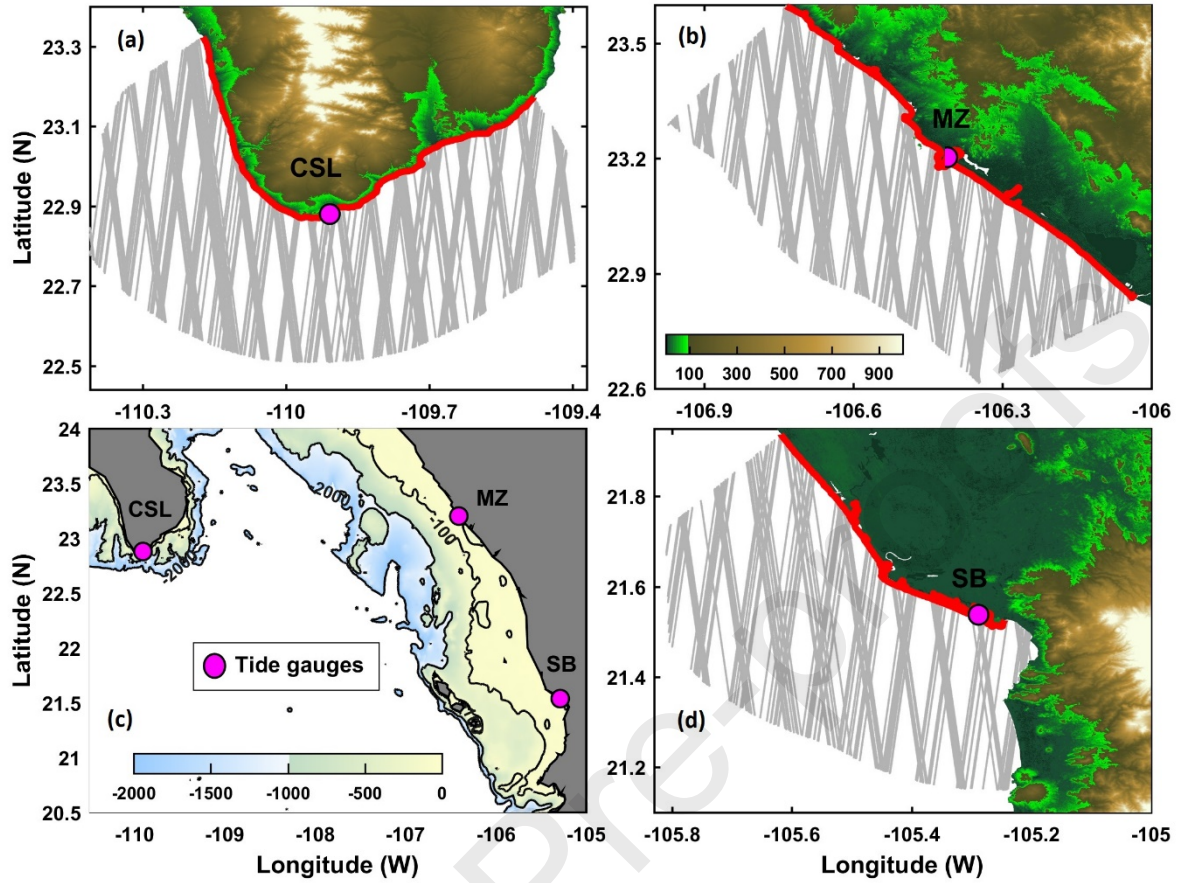


Figure 1. The entrance to the Gulf of California is shown in panel c. Tide gauges are represented as large purple circles. The bathymetry of the first 2000 meters is obtained from GEBCO. Panels a, b, and d show the enlarged areas around the tide gauges. The red line corresponds to the reference coastline. Gray lines are CryoSat-2 mission tracks. Terrain elevation is obtained from ASTER digital elevation model and plotted on a scale from green to brown.

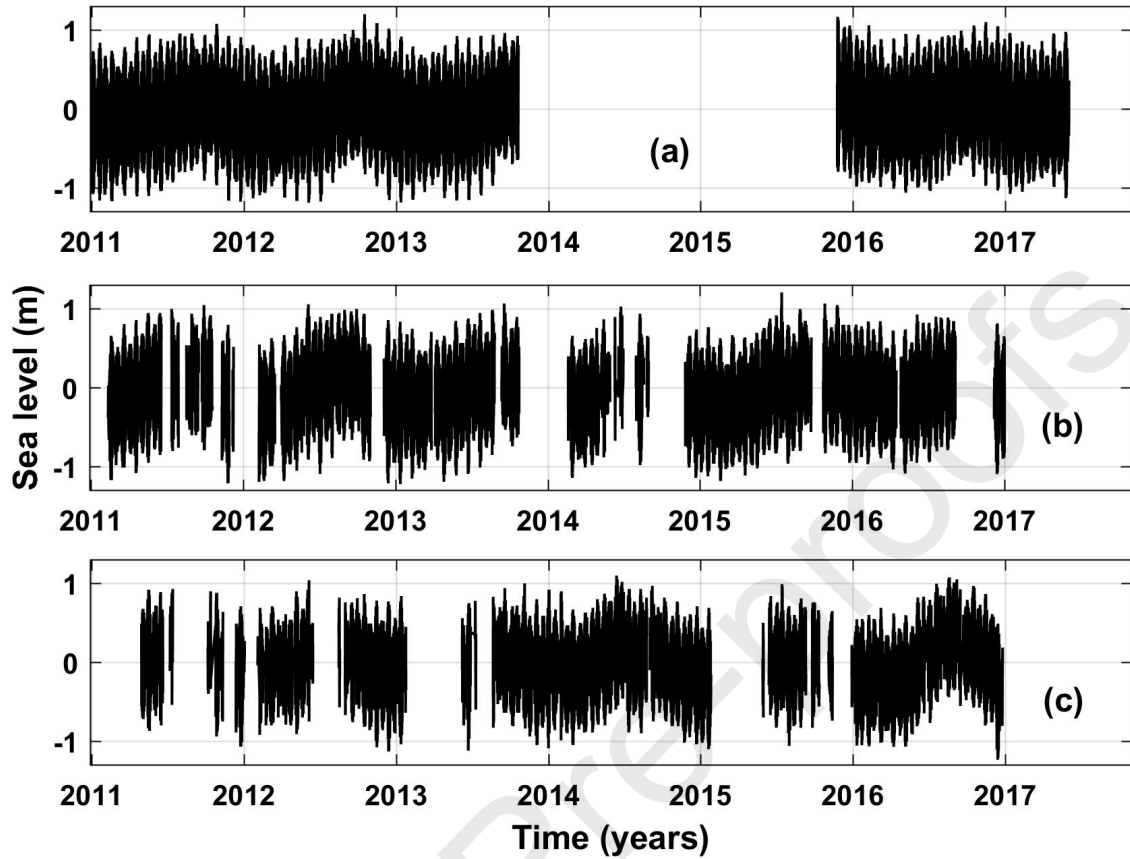


Figure 2. Sea level time series from tide gauges at the study area. Cabo San Lucas (a), Mazatlán (b) and San Blas (c).

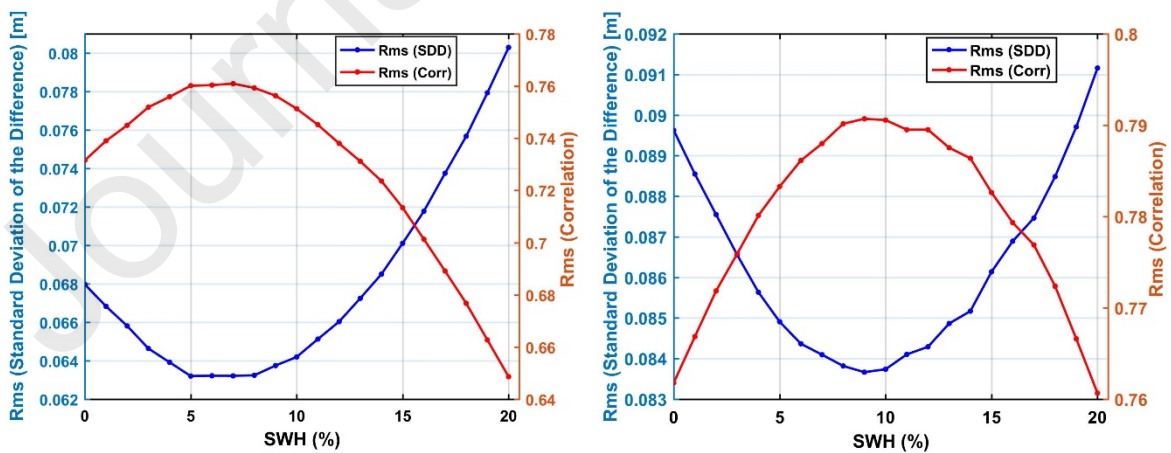


Figure 3. Root mean square of SDD (blue line) and correlation (red line) according to the percentage of SWH for Cabo San Lucas (left) and Mazatlán (right).

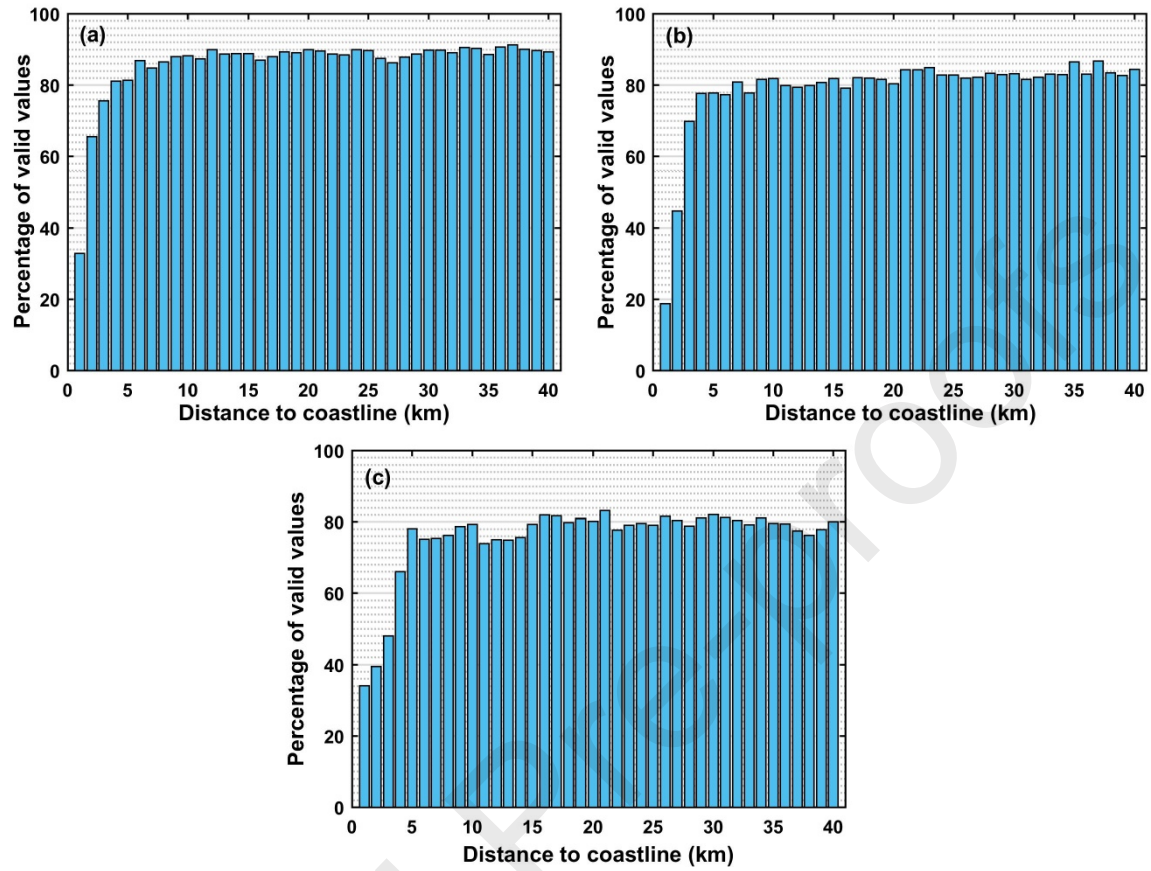


Figure 4. Percentage of SLA values with respect to the coastline after the two screening steps. For CSL (a), MZ (b), and SB (c).

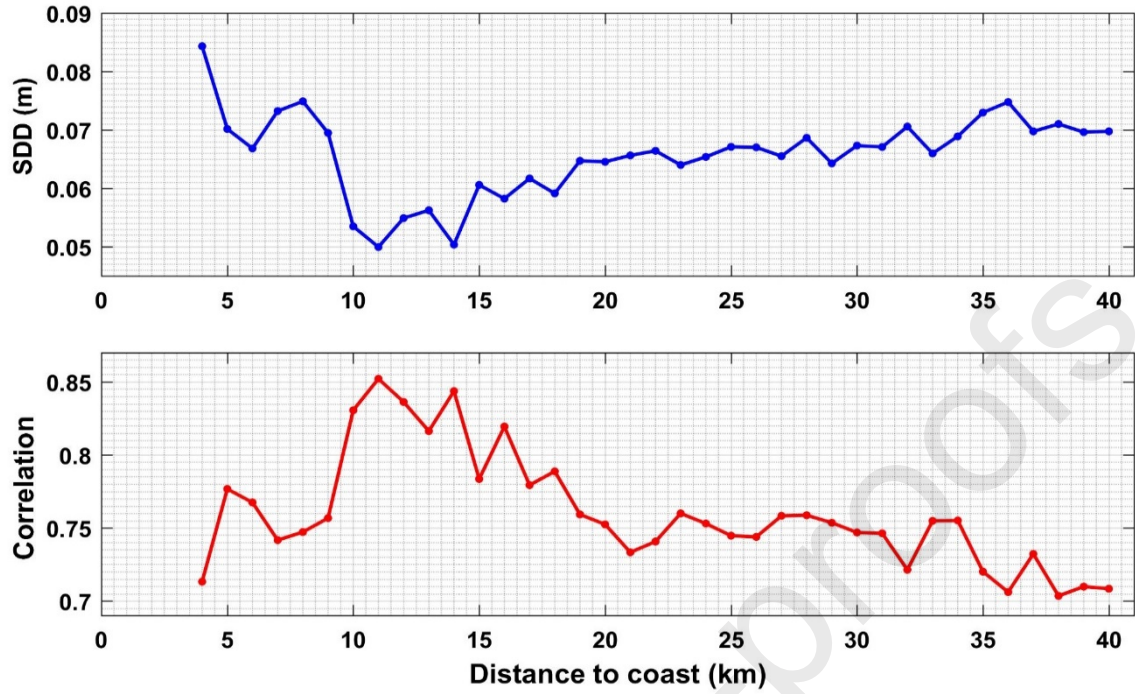


Figure 5. Standard deviation of the differences (SDD, top panel) and correlations (bottom panel) in CSL for the SLA_{CS2} and SLA_{TG} series with respect to the distance to the coast.

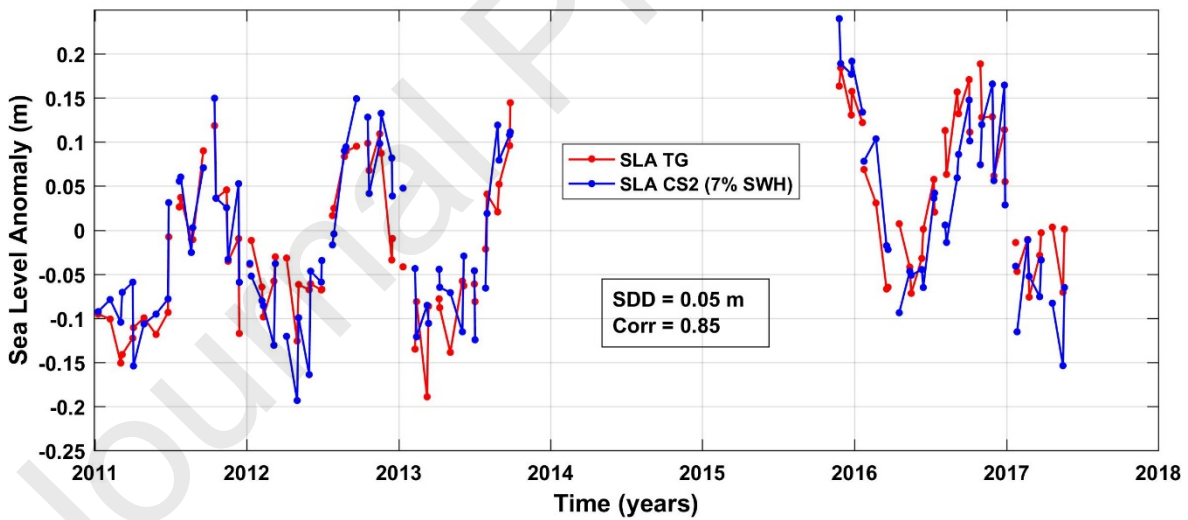


Figure 6. Sea level anomaly (SLA) series at CSL location. Tide gauge (red line) and CryoSat-2 (blue line) at 11 km with respect to the coastline.

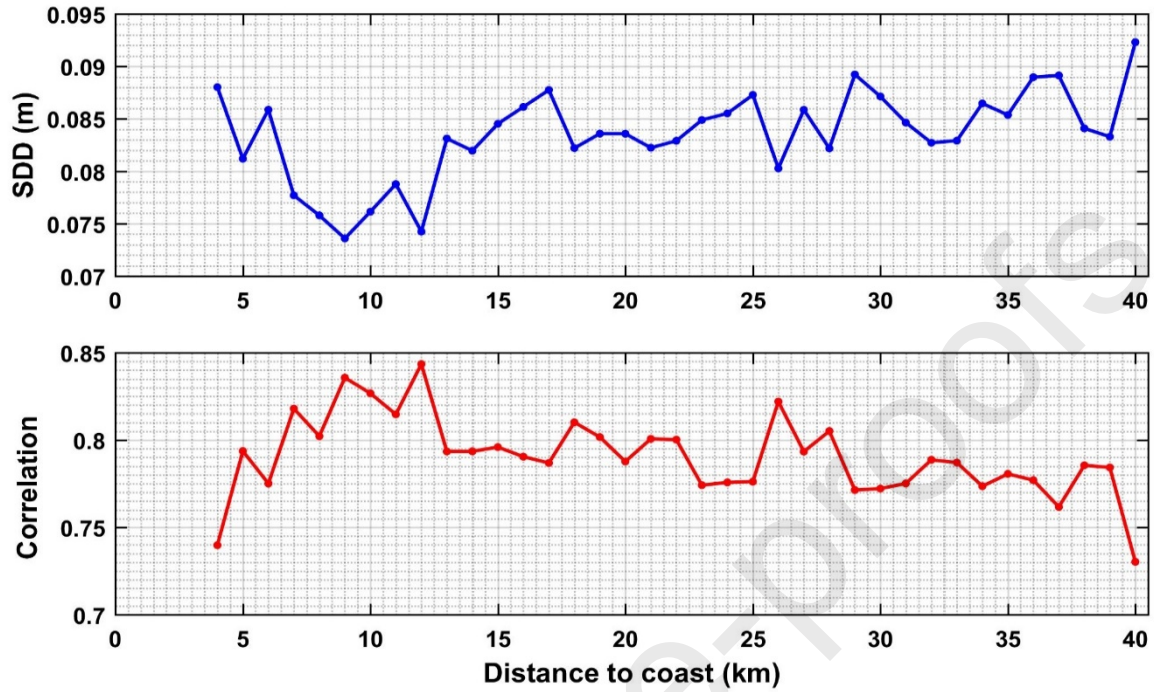


Figure 7. Same as Fig. 5 for MZ station.

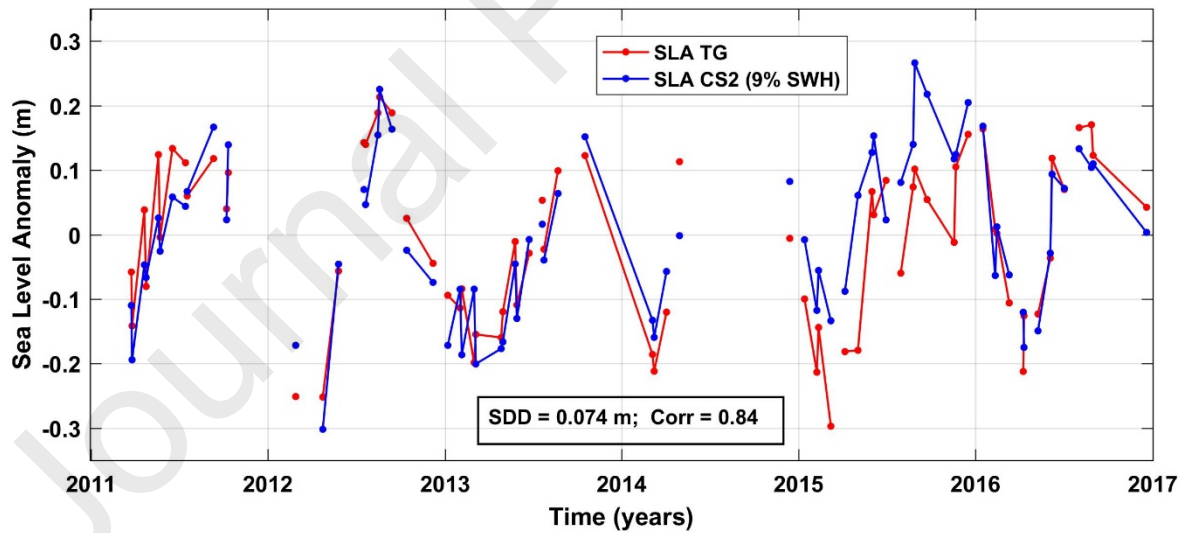


Figure 8. Sea level anomaly (SLA) series at MZ location. Tide gauge (red line) and CryoSat-2 (blue line) at 9 km with respect to the coastline.

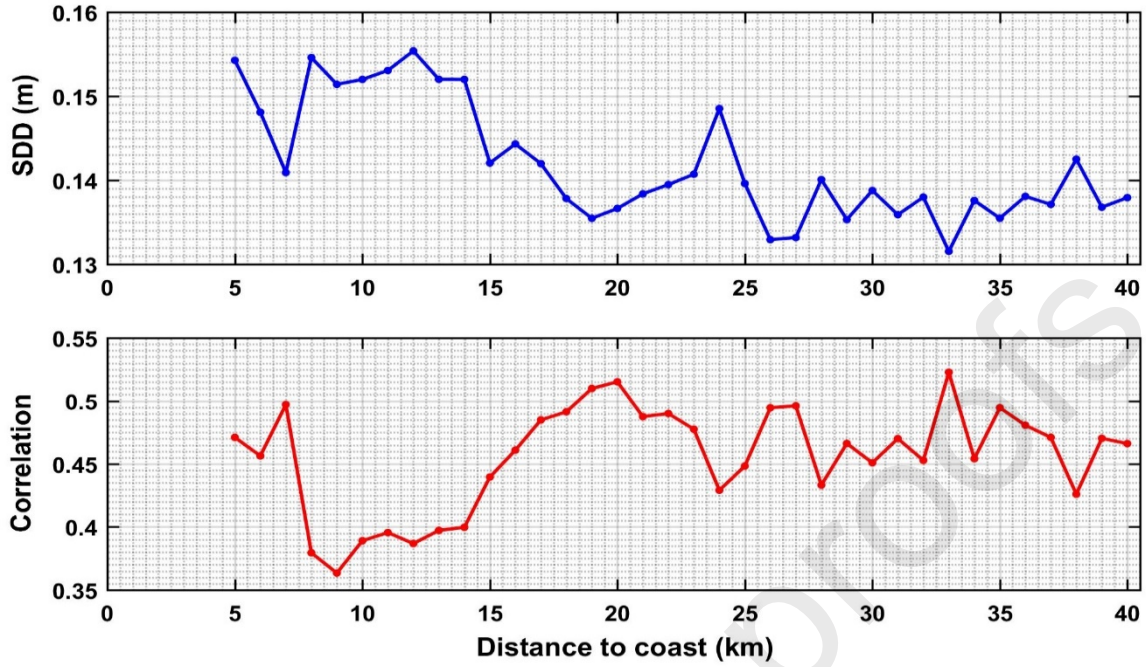


Figure 9. Same as Fig. 5 for SB station.

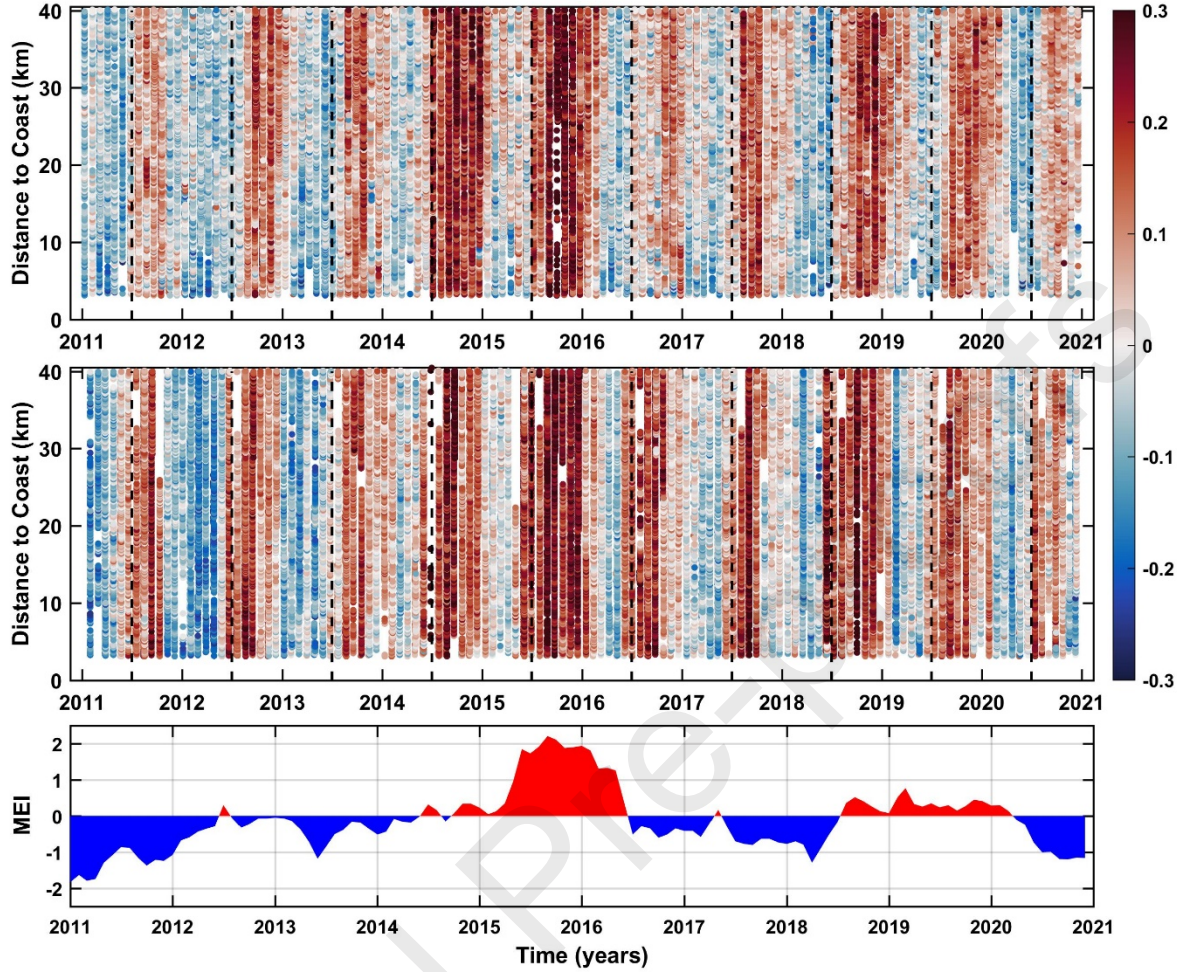


Figure 10. (top) Hovmöller diagram of SLA based on tracks around CSL. (middle) Similar to the top for MZ. The units of the colorbar are in meters. Dashed lines indicate the beginning of July. (bottom) Multivariate ENSO Index.

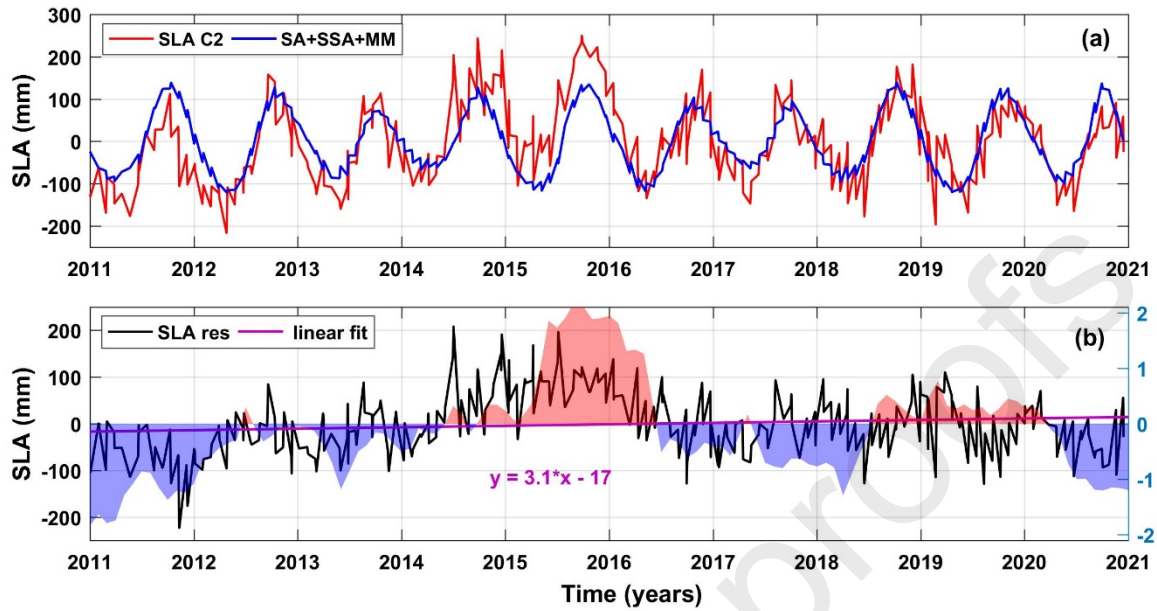


Figure 11. (a) Mean SLA for CSL (red line). Reconstructed signal of the annual, semi-annual and monthly harmonic (blue line). (b) Residual SLA (black line) and linear fit (purple line) the Multivariate ENSO Index is the shaded curve.

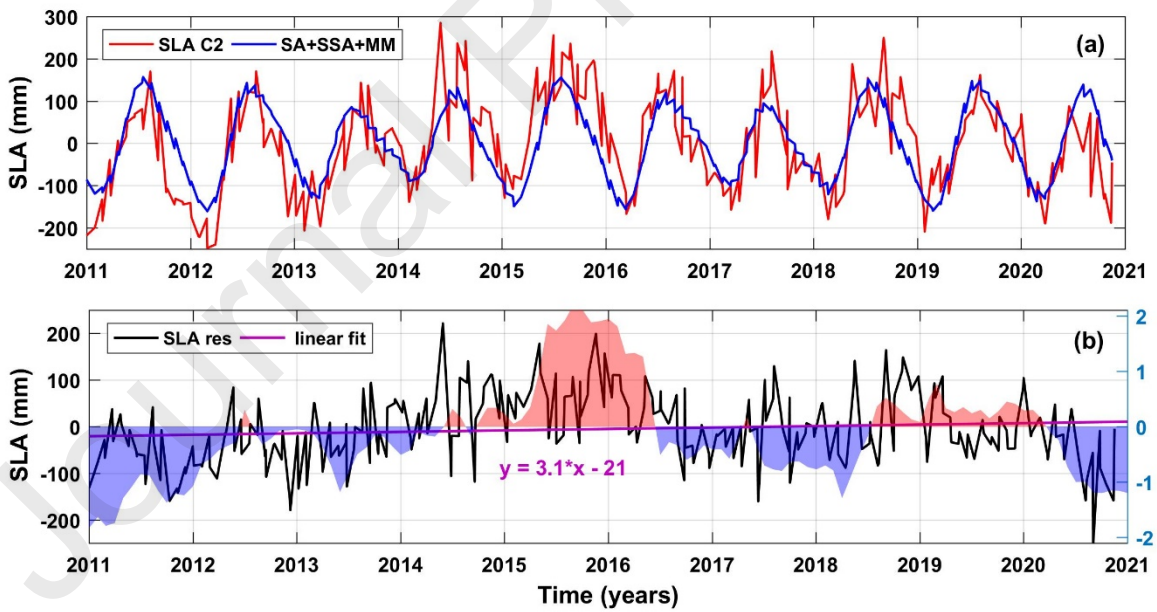


Figure 12. Same as Fig. 11 for MZ location.

Highlights

- LRM data from CryoSat-2(CS2) are useful in coastal areas of the Gulf of California (GOC).
- SLA from CS2 shows seasonal and interannual signals as El Niño/La Niña or the Blob.
- Estimated trends of CS2 at the entrance of GOC are close to global estimates.

Declaration of interests

The authors declare that they have no known competing financial interests or personal relationships that could have appeared to influence the work reported in this paper.

The authors declare the following financial interests/personal relationships which may be considered as potential competing interests:

Journal Pre-proofs